Electronic structure of $PbFe_{1/2}Ta_{1/2}O_3$: Crystallographic ordering and magnetic properties

Nathascia Lampis, Cesare Franchini, Guido Satta, Alessandra Geddo-Lehmann, and Sandro Massidda
Istituto Nazionale di Fisica della Materia (INFM) and Dipartimento di Scienze Fisiche, Università degli Studi di Cagliari, S.P. Monserrato-Sestu km 0.700, I-09124 Monserrato (Cagliari), Italy

(Received 13 July 2003; revised manuscript received 5 November 2003; published 13 February 2004)

We report electronic structure calculations for the multiferroic ferromagnetoelectric perovskite $PbFe_{1/2}Ta_{1/2}O_3$, within density functional theory in the local spin density approximation (LSDA) and within the LSD+U approach. Our results, corresponding to several possible crystallographic and magnetic orderings, show the link between short range cation coordination and magnetic properties. In particular, the existence of two different Néel ordering temperatures, experimentally evidenced, is explained in terms of different superexchange paths introduced by crystallographic orderings certainly present, locally, in the real samples. The introduction of ferroelectric displacements, which are found to be in good agreement with experiment, do not bring about large changes in the electronic structure of this system.

DOI: 10.1103/PhysRevB.69.064412 PACS number(s): 75.30.Et, 71.20.−b, 75.50.−y, 77.84.−s

I. INTRODUCTION

The term multiferroism was introduced[1] to describe the phenomenon in which at least two of the three properties ferroelectricity, ferromagnetism, and ferroelasticity occur in the same phase. In particular, multiferroics in which ferro(antiferro)electricity coexists with ferro(antiferro)magnetic order are called ferromagnetoelectrics,[2] a term coined in the thermodynamic classification of ferroics[3] to indicate materials in which the domain states differ in magnetoelectric coefficients. Ferromagnetoelectrics, therefore, represent materials in which magnetization can be induced by an electric field and electrical polarization by a magnetic field, which are precisely the direct[4] and inverse[5] magnetoelectric effects. Aside from its fundamental importance, the mutual control of electric and magnetic properties is of significant interest for applications in magnetic storage media, and opens up an additional degree of freedom in devices construction, for example enabling the creation of electronic components whose characteristics may be engineered to respond to applied magnetic fields.

The search for ferromagnetoelectrics among perovskite-type ferroelectrics ABO_3 began in Russia in the 1950s with the replacement of some of the diamagnetic (d^0) B cations by transition metal (d^n) species.[6–8] One of the first compounds synthesized in ceramic form was $PbFe_{1/2}Ta_{1/2}O_3$ (PFT),[8] in which magnetic Fe^{3+} ($3d^5$, $S=\frac{5}{2}$) and nonmagnetic Ta^{5+} ($5d^0$, $S=0$) share the B site of the perovskite structure. Only from the early 1990s have quantitative investigations of systems displaying simultaneous electric and magnetic order attracted the attention of density functional theory studies, whereas first principles calculations are, very sparse.[9–13]

PFT belongs to the wide family of complex Pb-based oxides with general formula $PbB'_{1/2}B''_{1/2}O_3$. The physics of such materials is known to be strongly influenced by the underlying chemical distribution of B cations on the octahedral sublattice of the perovskite structure. In particular, the existence of small B-site ordered regions (polar nanodomains) embedded in an otherwise B disordered matrix is the necessary ingredient for determining the glasslike or relaxor properties of ferroelectricity, one of the hot topics in the field during the past several years.[14]

The problem of B species ordering in complex Pb-based perovskites is well known.[15,16] Depending upon the electrostatic interaction between B′ and B″, different degrees of long-range order are realized.[16,17] For random distributions of B′ and B″, the cubic prototype, which is the parent structure from which all the derived ferroelectric or antiferroelectric phases can be obtained by small distortions, has symmetry $Pm\bar{3}m$ and a unit cell with a lattice parameter a_c of about 4 Å. A large difference in the valence states of B′ and B″ favors structural variants that are octahedrally ordered. In most cases an alternance of B′ and B″ along all the three Cartesian directions occurs, leading to a face-centered-cubic cell with double lattice parameter (the $Fm\bar{3}m$ elpasolite-type structure, which will be indicated as the $\frac{1}{2}(111)$ variant in the following). Complete long-range $\frac{1}{2}(111)$ octahedral order is observed in double perovskites $Pb_2B'^{2+}B''^{6+}O_6$ like Pb_2MgWO_6 and Pb_2CoWO_6,[18,19] that, consequently, do not show relaxor properties. In contrast, partial $\frac{1}{2}(111)$ long-range order is possible in $Pb_2B'^{3+}B''^{5+}O_6$ phases, in which the charge difference of B′ and B″ is smaller. The degree of order in real samples depends mainly on synthesis conditions.[20–22] Well ordered samples display normal ferroelectric phase changes, while, with increasing disorder, the transitions show the classical features of relaxors,[23–25] with broad Curie ranges and strong low-frequency dielectric dispersion in the transition range.

Among the $Pb_2B'^{3+}B''^{5+}O_6$ compounds, PFT is unique, together with the isostructural $PbFe_{1/2}Nb_{1/2}O_3$ (PFN),[26] in the sense that it can only be obtained in the completely long-range disordered form. Single crystals of PFT undergo two successive ferroelectric phase transitions that take place at about 270 and 220 K,[27,28] each one occurring in a quite narrow temperature range. The sequence of the ferroelastic/ferroelectric symmetry changes, defined by high-resolution x-ray diffraction and observations of oriented crystal sections in polarized light microscopy,[29] was defined as cubic ($Pm\bar{3}m$) → tetragonal (P4mm) → monoclinic (Cm), with

Fe and Ta randomly distributed over the octahedral sites in all the three phases.

Even if no sign of Fe^{3+} and Ta^{5+} order has been observed in the neutron and x-ray diffraction pattern,[28,29] the possible presence of nanoscale short-range ordered regions is still under discussion. The dielectric behavior shows, in fact, pronounced relaxor properties, with the two maxima of the dielectric constant, corresponding to the two structural transitions, displaced towards higher temperatures for increasing frequencies.[30,31] Signs of the possible existence of B-site ordered regions in PFT are also revealed in its magnetic properties. The magnetic susceptibility shows an antiferromagneticlike anomaly at a temperature which is strongly sample dependent, and equal to 133, 160, and 180 K according to different authors.[32–34] The magnetic structure was refined at 10 K from neutron powder diffraction data and is G-type antiferromagnetic, with the lattice parameter doubled with respect to the crystallographic $Pm\bar{3}m$ one, disregarding the weak ferroelectric pseudo–rhombohedral distortion.[35] The occurrence of G-type order is a feature common to PFT and to the isostructural PFN.[36] In the undistorted antiferromagnetic G-type structure, each magnetic $\frac{1}{2}Fe^{3+}$ ion, which shares with $\frac{1}{2}Ta^{5+}$ the octahedral site, interacts with its six nearest neighbors via oxygen-mediated 180° antiferromagnetic superexchange. As happens in PFN, also in PFT at 9 K there is experimental evidence of a second magnetic transition indicated by an anomaly in the magnetic field induced polarization.[30,37] Given the weakness of the magnetoelectric signal reported below 9 K, the hypothesis has been formulated[1] that it involves only that tiny volume fraction of B-site ordered clusters not revealed by those experimental techniques (like x-ray and neutron Bragg diffraction) which only probe average structural properties. The value of 9 K of the transition temperature (one order of magnitude smaller than the Néel point of the G-type phase) makes a strong case for the existence, in such clusters, of long superexchange paths of the kind Fe-O-Ta-O-Fe, with iron atoms about 8 Å apart, i.e., about twice the distance between iron moments in the G-type phase: transition temperatures of about 10 K characterize, in fact, the magnetic phases of ordered doubled perovskites $A_2B'B''O_6$ with one magnetic and one nonmagnetic B-type cation.[1,16] The question of which kind of B-site ordering scheme might be responsible for the low temperature magnetic behavior (as well as that of the relaxorlike features) of PFT, can be clarified by detailed theoretical studies of the properties of hypothetically ordered samples. The effects of B-site long range order on the structural and dielectric properties of Pb-based perovskites have been studied theoretically in the past years.[38–40] In this context, first-principle density-functional theory calculations have been used to understand the basic principles underlying ferroelectricity in these systems which, however, are not magnetic.

In this paper we investigate by first principle density functional calculations, using the local spin density (LSD) and (because of electron correlation) LSD+U approximations, the influence of B-site ordering on the structural, electronic and magnetic properties of $PbFe_{1/2}Ta_{1/2}O_3$. Several distributions of B′ and B″ over octahedral sites exist, giving rise to different superstructures of the disordered $Pm\bar{3}m$ phase. We take into consideration the elpasolite-type $\frac{1}{2}(111)$ and the $\frac{1}{2}(100)$ ordered variants, which are obtained by adding a B′:B″ layer sequence perpendicular to the $[111]_{cub}$ and $[100]_{cub}$ directions, respectively. This choice is suggested by the work of Gui *et al.*,[41] who studied the relative stability of different ordered variants in complex perovskites $AB'_xB''_{1-x}O_3$ by the eight-point cluster variation method (CVM). At the composition $x=\frac{1}{2}$, corresponding to PFT, the $\frac{1}{2}(111)$ and $\frac{1}{2}(100)$ variants were found to be the most stable.

The paper is organized as follows: in Sec. II we give the computational details. In Sec. III we discuss the choice of Coulomb and exchange interaction parameters used in the LSD+U calculation. In Sec. IV we discuss the magnetic properties of the chosen ordered models of PFT. In Sec. V we present the electronic properties and some considerations on ferroelectric distortions. Finally, conclusions are drawn in Sec. VI.

II. COMPUTATIONAL DETAILS

First principles density functional theory (DFT) calculations were performed using both the all-electron full-potential linearized augmented plane wave (FLAPW) method[42] and the Vienna *ab-initio* simulation package (VASP) (Ref. 43) within the projector augmented wave (PAW) method[44] as implemented by Kresse and Joubert,[45] within the local spin density approximation (LSDA) to the DFT in the Perdew-Zunger parametrization of the results of Ceperly and Alder.[46]

It is a well known fact that the conventional DFT-LSDA turns out to be inadequate in treating the electronic structure of materials with ions having partially filled *d* or *f* valence states. In particular, it has been shown that for many transition metal oxides the DFT-LSDA predicts a metallic ground states instead of the experimentally observed insulating ones. It is therefore necessary to use more sophisticated approaches[47] which include a better treatment of the on-site Coulomb repulsion. In this work we will use the LSD+U (Ref. 48) approach, implemented following the Shick formalism[49] in the FLAPW method and the scheme of Dudarev[50] in the VASP calculations. The consistency of the two implementations has been checked in the simple case of MnO, for which LSD+U FLAPW results are already available.[51]

In the case of PFT, as better explained in Sec. IV, big supercells are necessary to study the magnetic properties associated to different cationic orderings. Due to its high efficiency, VASP allows one to treat big cells within a reasonable computing time, in contrast to a pure all-electron full-potential method that requires a much larger effort. We first checked the accuracy of VASP calculations by comparing the structural, magnetic, and electronic properties obtained by VASP and FLAPW methods within the LSD and LSD+U approximations on the smallest cell among those described in Sec. IV. In order to minimize the computational time we then proceeded in our investigations of bigger cells using only the PAW-VASP scheme.

In FLAPW calculations well converged results were obtained using plane waves in the interstitial region with a wave vector up to $k_{max}=3.5$ a.u.. We used the muffin-tin (MT) sphere radii $R_O=1.5$ a.u., $R_{Fe}=2.2$ a.u., $R_{Ta}=2.1$ a.u., and $R_{Pb}=2.3$ a.u.. The LAPW wave functions within the MTs were expanded in spherical harmonics with angular momentum up to $l_{\max}=8$. The nonspherical contribution to the charge density and the potential within the MTs were expanded in lattice harmonics including all terms with $l_{max}\leqslant 8$. The core electrons were treated fully relativistically and the valence electrons semirelativistically, i.e., neglecting only the spin-orbit term in the Hamiltonian. The Brillouin zone integration was performed using a $4\times4\times4$ Monkhorst-Pack type mesh, that turned out to be sufficiently accurate for the present purposes. The accuracy of this mesh was checked by comparison with results obtained with $8\times8\times8$ inequivalent *k* points used to compute the densities of states (DOS).

For the VASP calculations an energy cutoff of about 280 eV and the same *k*-point meshes described above were used. To improve the *k*-point sampling convergence, a Gaussian smearing with an electronic temperature of 0.2 eV was used and the DOS was computed using the tetrahedron method. We used valence electron configurations $3d^74s^1$, $5d^{10}6s^2p^2$, $5p^6s^25d^3$, and $2s^2p^4$ for the Fe, Pb, Ta, and O pseudopotentials, respectively.

III. PARAMETERS OF COULOMB AND EXCHANGE INTERACTION

Before discussing our results, a few comments on the values adopted for the on-site Coulomb interaction *U* and the Hund's rule exchange parameter *J* for Fe ions are needed. It is still difficult to find a correct procedure to evaluate *U* and *J* for compounds,[52] and the parameters used in literature may be very different. There is no agreement even in the simple case of FeO, for which the various values of *U* estimated by different approaches range from 3.9 (Ref. 53) and 7.0 eV.[54,55]

As a general rule *U* decreases with decreasing transition metal atomic number, due to the increase in the spatial extent of the *d* orbitals.[55] This is true, for instance, for transition metal perovskites of the series RMO_3 (R=rare earth or Y and $M=M$=Ti-Cu), for which U ranges from 6.5 (Ti) and 8.5 (Cu), and from 8.0 (Ti) and 10.0 (Cu) for a divalent (M^{2+}) and trivalent (M^{3+}) configuration of the transition metal ions respectively.[55–58] Also for double transition metal perovskites of the series $A_2MM'O_6$ (A=Ba, Sr, Ca, M=Ti-Co and M'=Mo, W and Re) *U* values range from medium/strong correlation ($U=3.0$) to strong ($U=5.0$) $3d$ electron-electron interaction.[59–61]

The origin of the efficient screening of one extra *d* electron in perovskites has been widely discussed under the assumption of an itinerant character of the e_g electrons, which are therefore allowed to participate in screening the localized electronic states of t_{2g} symmetry.[56] For PFT, the Fe magnetic moment obtained by magnetic susceptibility measurements is $4.7\mu_B$,[34] which, in the spin-only approximation, is in quite good agreement with a localized picture of both t_{2g} and e_g electrons of the iron $t_{2g}^3e_g^2$ electronic configuration. Therefore, a situation can be envisaged in which, as it happens in $LaFeO_3$,[56] all $3d$ electrons are unscreened and feel a large Coulomb interaction.

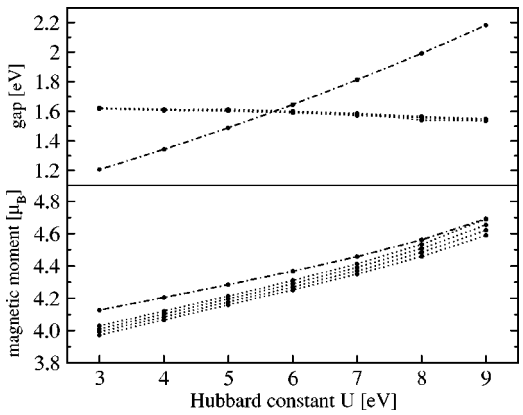

FIG. 1. Calculated Fe magnetic moment and energy gap vs Hubbard-like interaction parameter *U* for the $\frac{1}{2}(100)$ C-type (full line) and $\frac{1}{2}(111)$ G-type (dashed line) structures of PFT. For each *U* value the four displayed points corresponds to the exchange parameter *J* equal to 0.2, 0.4, 0.6, and 0.8 eV from bottom to top. For the $\frac{1}{2}(111)$ variant we only display the results obtained for $J=0.8$ eV.

To make a reasonable choice of *U* and *J*, we made a preliminary investigation of their influence on some of the calculated electronic and magnetic properties. More in details, we calculated, both in the variant $\frac{1}{2}(100)$ (in the C-type magnetic order; see Sec. IV for details about magnetic structures), and in the variant $\frac{1}{2}(111)$ (type-I magnetic order, also described in details in the next section), the Fe magnetic moment μ_B and the band gap E_g for the Hubbard-like parameter *U* between 3.0 and 9.0 eV and for *J* between 0.2 and 0.8 eV. The results are reported in Fig. 1.

For a fixed value of U, both quantities have only a minor dependence on *J*. An insulating ground state is predicted for all *U* values. The behavior of the gap is different for the two crystallographic variants. In the $\frac{1}{2}(100)$ case the energy gap remains almost unchanged for all the *U* values considered. In the $\frac{1}{2}(111)$ case, on the other hand, we have a linear dependence of E_g on *U*. This difference will be clarified later on by the analysis of the densities of states. As expected, the magnetic moment of Fe increases monotonically with increasing *U* for both variants, reaching the experimental value at $U=9.0$ eV. The moment is slightly larger in the $\frac{1}{2}(111)$ variant for small values of *U* and the slope is correspondingly smaller. It should be remarked that in the present case the comparison with experiment cannot conclusively dictate a particular value of *U*, due to the disorder present in the experimental case. However, the dependence of the Fe magnetic moment on the ordering is not dramatic (within $0.1\mu_B$). On the other hand, *U* values smaller than 9 eV lead to magnetic moments significantly smaller than the experimental one, and in the absence of a better criterion we decided to use in all calculations the value of *U* which gives the magnetic moment in better agreement with the experimental value. The value of *J* was fixed at 0.8 eV, which is typical of the transition metal oxides, where it varies between 0.78 and 0.98 eV.[62]

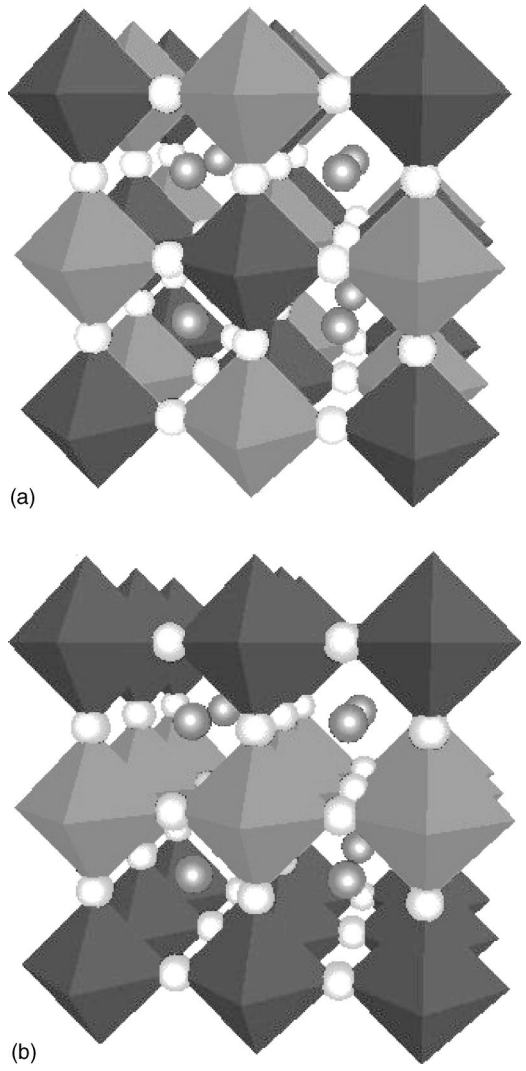

FIG. 2. Crystallographic ordered structures chosen for $PbFe_{1/2}Ta_{1/2}O_3$. Fe octahedra are dark gray, Ta octahedra are light gray, O atoms are white spheres, and Pb atoms are the gray ones. (a) $\frac{1}{2}(111)$ variant. (b) $\frac{1}{2}(100)$ variant.

IV. CRYSTALLOGRAPHIC ORDERING AND MAGNETIC PROPERTIES

The two ordered structure considered for PFT are shown in Fig. 2. As mentioned above, in the $\frac{1}{2}(111)$ variant [Fig. 2(a)] the alternance along the three cubic directions produces a doubling of the cell parameters with respect to the paraelectric $Pm\bar{3}m$ prototype. In the following we name the planar oxygen sited in the *xy*-Fe/Ta planes O1 and the apical oxygen, coplanar with Pb atoms, O2. The resulting symmetry is cubic $Fm\bar{3}m$. In the $\frac{1}{2}(100)$ model [Fig. 2(b)], sheets of Fe and Ta octahedra alternate along the *z* axis, doubling the cell only in one direction. As a consequence there are two kinds of planar oxygens, O1a and O1b, the former sited in the Fe planes, the latter in the Ta planes. The symmetry is tetragonal P4/mmm.

A. Antiferromagnetism in the $\frac{1}{2}(100)$ variant

In the $\frac{1}{2}(100)$ structural variant, Fe magnetic moments are located on a simple-tetragonal lattice with axial ratio c/a of about two [cf. Fig. 2(b)]. Short and long 180° superexchange paths like Fe-O-Fe and Fe-O-Ta-O-Fe connect, respectively, a Fe atom to four in-plane and two interplane nearest neighbors with exchange integrals indicated in the following as J_1^s and J_2^s, where superscript *s* means superexchange. Each Fe atom also interacts with four in-plane second nearest neighbors trought a diagonal direct exchange interaction (i.e.: without intervening anion) which we indicate as J_d.

To model the exchange interactions of the system of Fe^{3+} magnetic moments, we start from the Heisenberg spin Hamiltonian

$$H_{ex} = -\sum_{i,j} J_{i,j}\mathbf{S_i}\cdot\mathbf{S_j}, \tag{1}$$

in which $J>0$ for ferromagnetic exchange and $J<0$ for the antiferromagnetic case. The values of the exchange parameters can be obtained by total energy differences of different magnetic configurations, with the number of necessary magnetic states determinated by the number of exchange constants in Eq. (1).

At first we restrict ourselves to the case of J_1^s and $J_2^s \neq 0$ and $J_d = 0$, i.e., we describe the antiferromagnetic behavior of PFT in terms of exchange interactions mediated by anions. Among possible magnetic cells we take into consideration the case of in-plane antiferromagnetic ($J_1^s<0$) and interplane ferromagnetic ($J_2^s>0$) couplings and the case of both exchange interactions antiferromagnetic (J_1^s, $J_2^s<0$). For analogy with the simple cubic lattice, the two structures will be indicated as antiferromagnetic C and G types, respectively. The magnetic cells used in calculations are shown in Fig. 3. Both correspond to space group P4/mmm and are rotated by 45° with respect to the crystallographic cell [cf. Fig. 2(b)]. The C-type cell [Fig. 3(a)] has dimensions $a=b=a_c\sqrt{2}$ and $c=2a_c$, where a_c is the cubic parameter of the $Pm\bar{3}m$ disordered structure. In the G-type cell [Fig. 3(b)] the antiparallel interplanar spin coupling produces a doubling of the *c* tetragonal parameter.

Neglecting quantum fluctuations we can write the following expressions for the total ferromagnetic (E_F) and antiferromagnetic (E_{AF}) energies:

$$E_F = E_{nm} - 4J_1^s S^2 - 2J_2^s S^2, \tag{2}$$

$$E_{AF}^C = E_{nm} + 4J_1^s S^2 - 2J_2^s S^2, \tag{3}$$

$$E_{AF}^G = E_{nm} + 4J_1^s S^2 + 2J_2^s S^2, \tag{4}$$

where E_{nm} is the non magnetic part of the total energy and the superscripts *C* and *G* refer to the C- and G-type structures. Energies are calculated per *f.u.* containing one Fe atom.

From Eqs. (2)–(4) we get, for the exchange integrals,

$$J_1^s = \frac{1}{8S^2}(E_{AF}^C - E_F), \tag{5}$$

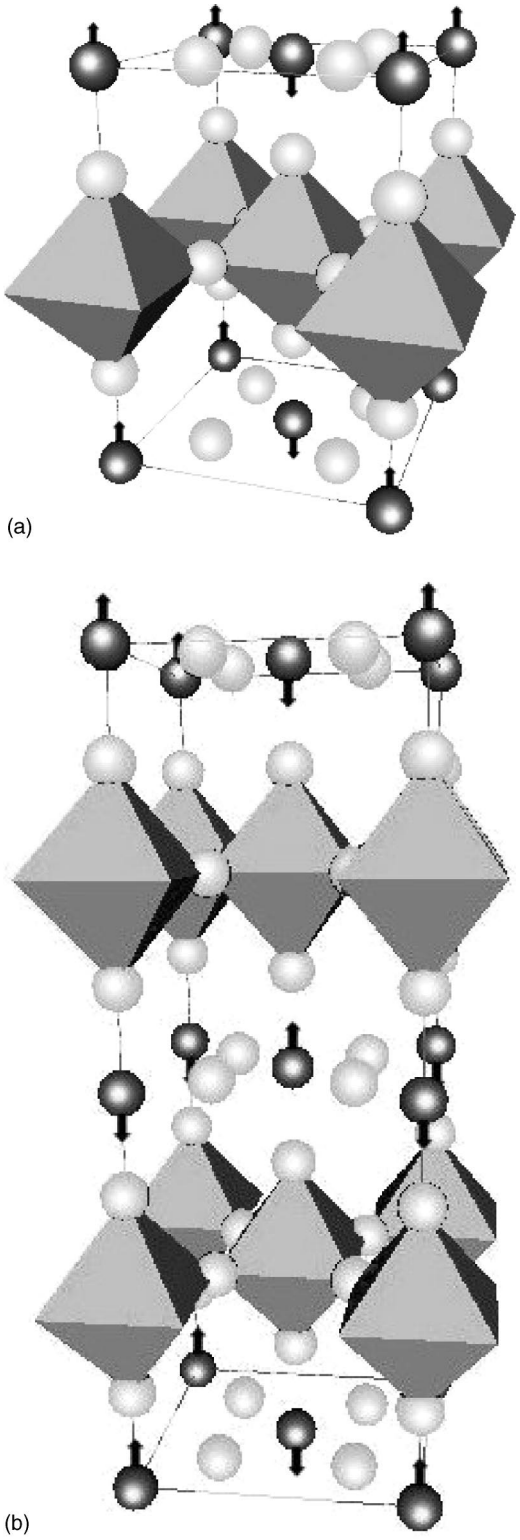

FIG. 3. Magnetic $\frac{1}{2}(100)$ structures. Fe and O atoms are represented by dark and white spheres, respectively. Ta octahedra are shown for better visualizing the long superexchange paths F-O-Ta-O-Fe along the *z* direction. Pb atoms are not shown. (a) C-type cell. (b) G-type cell.

$$J_2^s = \frac{1}{4S^2}(E_{AF}^G - E_{AF}^C). \tag{6}$$

From the knowledge of J_1^s and J_2^s, the Néel transition temperatures can be evaluated from the molecular field formulas:

$$T_{Néel}^{C\text{-}type} = \frac{2S(S+1)}{3k_B}(-4J_1^s + 2J_2^s), \tag{7}$$

$$T_{Néel}^{G\text{-}type} = \frac{2S(S+1)}{3k_B}(-4J_1^s - 2J_2^s). \tag{8}$$

In a second step the effect of the in-plane diagonal interaction J_d has been considered. To this end a further in-plane nonfrustated magnetic configurations was taken into account, consisting of Fe rows along the [010] cubic direction with an antiferromagnetic inter-row alignment and with ferromagnetic in-row and inter-plane coupling. With the direct in-plane interaction taken into account, the term $-4J_dS^2$ has to be added to the total energies in Eqs. (2)–(4), while the total energy of the new model (in the following named Row model) is written as

$$E^{Row} = E_{nm} - 2J_2^s S^2 + 4J_d S^2. \tag{9}$$

From the new equations it is possible to evaluate the three exchange parameters J_1^s, J_2^s, and J_d. In particular J_1^s and J_2^s remain unchanged and the diagonal exchange parameter J_d is given by

$$J_d = \frac{1}{16S^2}(2E^{Row} - E_F - E_{AF}^C). \tag{10}$$

The changes in the transition temperatures due to J_d are straightforward: in Eqs. (7) and (8) the contribution $+4J_d$ of the in-plane second neighbors has to be added in parenthesis.

Before proceeding in our analysis, in order to check the reliability of the above formalism and the accuracy of our calculations we have calculated J_1^s and $T_{Néel}^{G\text{-}type}$ for $LaFeO_3$, for which both experimental[63,64] and theoretical results[65] are available in literature. We find $E_{AF}^G - E_{FM} = 161$ meV, very close to the experimental value of 147 meV.[65] Our result leads to $J_1^s = 2.15$ meV, in good agreement with the experimental finding of 2.27 meV. For the Néel temperature we obtain the value of 873 K, to be compared with the experimental result of 740 K.

B. Antiferromagnetism in the $\frac{1}{2}(111)$ variant

In the crystallographic variant $\frac{1}{2}(111)$, the B sublattice can be recognized to form a rocksaltlike structure, in which each kind of cation Fe^{3+} and Ta^{5+} lies on its own face-centered-cubic lattice. Antiferromagnetism in three-dimensional fcc systems is discussed[66] in terms of the relative number of ferromagnetic and antiferromagnetic interactions involving nearest (nn) and next-nearest (nnn) magnetic neighbors, with exchange coupling constants J_1^s

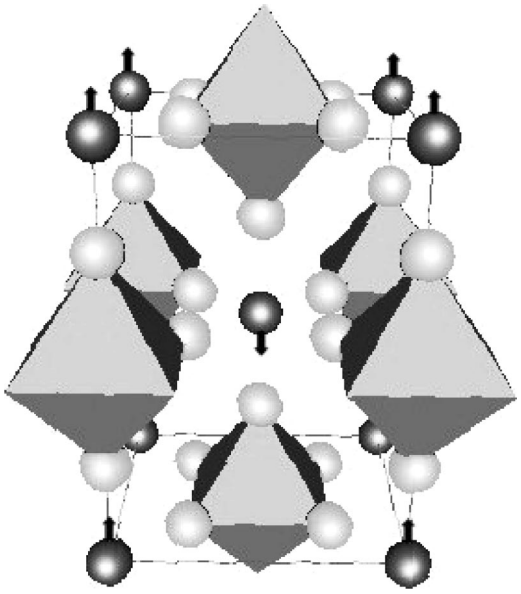

FIG. 4. Type-I $\frac{1}{2}(111)$ antiferromagnetic structure. Fe and O atoms are represented by dark and white spheres, respectively. Nonmagnetic Ta octahedra are shown. Pb atoms are not shown.

and J_2^s, respectively. The type-I structure is formed by atomic moments coupled ferromagnetically in (100) planes, with antiferromagnetic interplanar coupling. The type-II arrangement consists of atomic moments coupled ferromagnetically in (111) planes, with adjacent planes still having antiparallel spins. In the type-I arrangement, two-thirds of nearest-neighbor pairs of magnetic moments are aligned antiferromagnetically, while the remaining nearest neighbors and all the next-nearest neighbors are coupled ferromagnetically. In the type-II structure, there are equal numbers of ferromagnetically and antiferromagnetically aligned nearest neighbors, while all next-nearest neighbors are aligned antiferromagnetically. The superexchange between next-nearest neighbors Fe^{3+} takes place via 180° Fe-O-Ta-O-Fe paths along $\langle 100\rangle_{cub}$, while nearest neighbors are coupled via 90° superexchange. Other spin ordering schemes, possible for the fcc lattice with only J_1^s and J_2^s interactions, e.g., those described by Hines *et al.*,[67] will not be taken into consideration in the present work. The type-I and -II antiferromagnetic structures are displayed in Figs. 4 and 5. The type-I cell (Fig. 4) is constructed on the same crystallographic axes used for the C-type $\frac{1}{2}(100)$ spin arrangement. The type-II magnetic structure (Fig. 5) has rhombohedral symmetry with the threefold axis along the [111] cubic direction. The rhombohedral lattice parameters are related to the B-site disordered cubic one as $a_r = 2a_c\sqrt{2}$ and $\alpha_r = 60°$. The magnetic cell has twice the volume of the crystallographic elpasolite cell [cf. Fig. 2(a)].

The relative stability of the type-I and -II structures is determinate by the ratio between $|J_1^s|$ and $|J_2^s|$. The type-II ground state would be destabilized by increasing the magnitude of the *nn* ferromagnetic coupling (characterized by a positive J_1^s) and stabilized by increasing the magnitude of antiferromagnetic *nnn* coupling (characterized by a negative J_2^s). The type-II order is stable, for the classical ($S\to\infty$) case

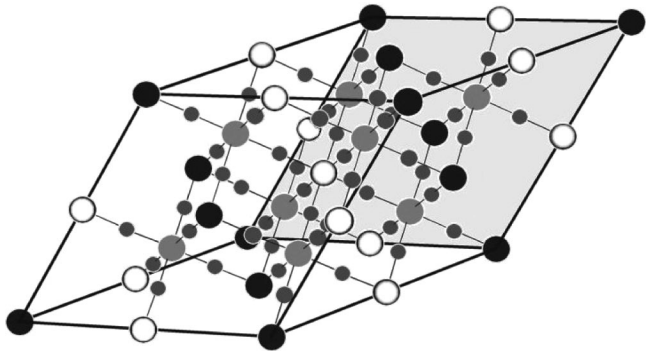

FIG. 5. Type-II $\frac{1}{2}(111)$ antiferromagnetic structure. Black and white circles indicate spin up and spin down Fe atoms, respectively. Ta atoms are gray. Small spheres are O atoms. Pb is not shown.

for $|J_1^s| < 2|J_2^s|$.[68,69] In the limit case $J_1^s \to 0$, the system goes over to the simplest of all the three-dimensional antiferromagnets (the G-type simple-cubic structure with a single J_2^s antiferromagnetic exchange parameter), while for $|J_1^s| = 2|J_2^s|$ long range order sets in only at 0 K, i.e., there is no phase transition at any finite temperature.

The evaluation of the exchange integrals from total energies in fcc magnetic lattices has already been treated in the case of transition-metal simple oxides NiO and MnO.[70,71] From the Heisenberg Hamiltonian (1) the following expressions exchange integrals were obtained:

$$J_1^s = \frac{1}{16S^2}(E_{AF}^I - E_F), \tag{11}$$

$$J_2^s = \frac{1}{48S^2}(4E_{AF}^{II} - 3E_{AF}^I - E_F). \tag{12}$$

Here again energies are calculated per Fe atom and superscripts *I* and *II* refer to types-I and -II. The Néel temperatures, evaluated from the molecular field formulas, are

$$T_{Néel}^{Type\text{-}I} = \frac{2S(S+1)}{3k_B}(-4J_1^s + 6J_2^s), \tag{13}$$

$$T_{Néel}^{Type\text{-}II} = \frac{2S(S+1)}{3k_B}(-6J_2^s). \tag{14}$$

C. Results

As starting point for all calculations, the five magnetically ordered structures of PFT were constructed with atomic positions derived from the ideally cubic perovskite and lattice parameters fixed at the experimental value $a_c = 4.0097$ Å of cubic PFT at 350 K.[28] As a first step, total energies were minimized against lattice constants, both in LSD and LSD+U approximations for the two ordered crystallographic variants in the C-type and type-I antiferromagnetic structures. With respect to the experimental volume, the calculated structures were found to be slightly contracted as reported in Table I. The smaller values found within LSD are not surprising. The LSDA+U approach still gives a value

TABLE I. Compilation of calculated lattice constants of PFT for both the $\frac{1}{2}(100)$ and $\frac{1}{2}(111)$ structural variants within the LSD and LSD+U approximations. The experimental values for the octahedrally disordered phase are taken from Ref. 28. All values are in Å.

	LSD	LSD+U		Exp.
	$\frac{1}{2}(100)$	$\frac{1}{2}(100)$	$\frac{1}{2}(111)$	
a	5.536	5.603	5.575	5.671
c	7.737	7.847	7.838	8.019

smaller than experiment, but the agreement within 2% is improved. Clearly, a detailed quantitative comparison with experiment should take into account the disorder present in the real samples. However, the difference between the $\frac{1}{2}(100)$ and $\frac{1}{2}(111)$ lattice constants is negligible ($\approx 0.6\%$). With the lattice constants so obtained, the energies of the five magnetic structures were minimized against atomic positions, which were varied under centro-symmetric (i.e., nonferroelectric) constraints.

The LSD+U total energies of the C-type, G-type, row-type, type-I and type-II magnetic structures for ordered $PbFe_{1/2}Ta_{1/2}O_3$, are given in Table II. The exchange parameters evaluated from Eqs. (5), (6), (10), (11), and (12) are reported in Table III. The direct exchange parameter J_d is found to be one and two orders of magnitude smaller than the superexchange parameters in the $\frac{1}{2}(100)$ variant and its contribution to the calculated Néel temperatures is very small (6 K). The Néel temperatures, estimated from Eqs. (7) and (8) (including the contribution due to J_d) and Eqs. (13) and (14) are reported in Table IV. We notice that the calculated Néel temperatures for the type-I and row models turn out to be negative, implying that they are not stable antiferromagnetic phases.

In the following we shall discuss how the obtained results allow us to explain the presence of the two different Néel temperatures measured in PFT. First of all, we note that the $\frac{1}{2}(100)$ and $\frac{1}{2}(111)$ variants are characterized by Néel temperatures differing by one order of magnitude. This immediately suggests to relate them to the high (160 K) and to the low (9 K) experimental Néel points found in PFT. The presence of short superexchange paths in the $\frac{1}{2}(100)$ case and its absence in the $\frac{1}{2}(111)$ structure shows the correlation existing between the Néel temperature and local cationic ordering. Accordingly, the calculated next nearest neighbors superexchange parameter J_2^s has the same value in the two ordered variants, as expected, since it refers to the same linear Fe-O-Ta-O-Fe exchange path. On the other hand J_1^s is much stronger for the short 180° superexchange paths of the $\frac{1}{2}(100)$ variant and is decisive for its higher values of T_N. We note that the value obtained for J_1^s (1.18 meV) for the Fe-O-Fe path is comparable with the measured[63,64] and calculated[65] exchange integrals for $LaFeO_3$, 2.27 meV and 1.96 meV (2.15 meV in our calculation), respectively.

TABLE III. LSD+U calculated exchange parameters for the magnetic structures of ordered $PbFe_{1/2}Ta_{1/2}O_3$. Energies are given in eV.

	$\frac{1}{2}(100)$		$\frac{1}{2}(111)$
J_1^s (meV)	−1.80	J_1^s (meV)	−0.04
J_2^s (meV)	−0.12	J_2^s (meV)	−0.12
J_d(meV)	−0.02		

In the $\frac{1}{2}(111)$ variant, with the lower Néel temperature, the calculated ratio J_1^s/J_2^s (cf. Table IV) indicates that the stable antiferromagnetic structure for an hypothetically elpasolite-type PFT is type II. The relatively high value of the calculated Néel temperature of this phase (48 K; cf. Table IV) compared to the experimental value of 9 K, can be ascribed to the use of molecular field formulas (11)–(14), in which fluctuations of the order parameter are neglected. Furthermore, the total energy differences between the magnetic structures for the $\frac{1}{2}(111)$ variant are very small, which makes a reliable quantitative estimation of T_N quite difficult. Also the possible influence of a size effect on the measured critical temperature should be considered, because of the small dimensions of the ordered domains in real samples. We also note that any elpasolite-type domain in real sample is expected to be ferroelectrically polarized, while our calculations are performed in cubic symmetry. We will discuss this point in Sec. V A. In our opinion, the previous results support the hypothesis that ordered $\frac{1}{2}(111)$ domains exist in the otherwise octahedrally disordered samples of PFT. As a matter of fact, a recent x-ray structural analysis claims,[31] in contrast to all the previous studies, the observation of weak superstructural reflections tentatively ascribed to partial $\frac{1}{2}(111)$ ordering of Fe and Ta (with an order parameter not exceeding 0.2).

We notice that, among the two magnetic mechanisms active in a double perovskite, double exchange and superexchange, it is the latter that determines the magnetic behavior of insulating $\frac{1}{2}(111)$ PFT. This is in contrast with the properties of other double perovskites in which magnetic interac-

TABLE II. Total energies of $PbFe_{1/2}Ta_{1/2}O_3$ calculated using the LSD+U approximation, for the antiferromagnetic and ferromagnetic structures taken into consideration. Energies are given in eV per Fe atom.

	$\frac{1}{2}(100)$			$\frac{1}{2}(111)$	
	C-type	G-type	Row model	Type-I	Type-II
E_{AF}	−80.24818	−80.25120	−80.204477	−80.16892	−80.17758
E_F		−80.15842		−80.16560	

TABLE IV. Néel temperatures (T_N), calculated in LSDA+U according to Eqs. (7) and (8) (including the contribution of J_d; see the text) and Eqs. (13) and (14), and Fe magnetic moments (μ), for the magnetic structures of ordered $PbFe_{1/2}Ta_{1/2}O_3$.

	$\frac{1}{2}(100)$		$\frac{1}{2}(111)$	
	C-type	G-type	Type-I	Type-II
T_N(K)	466	498	−38	48
μ (μ_B)	4.6	4.6	4.7	4.6

tions are dominated by double exchange, as for instance in the half-metallic ferrimagnetic Sr_2FeMoO_6 and Sr_2FeReO_6.[60,72] In this case the exchange integrals, proportional to the bandwidth of itinerant states, are found to be one and two orders of magnitude bigger than those found in our work for PFT. Correspondingly, the critical temperature for the half-metallic ferrimagnetics (about 401 K) are much bigger than the Neel point of the isostructural $\frac{1}{2}(111)$ PFT (experimentally 9 K, calculated 48 K).

As for the $\frac{1}{2}(100)$ variant, the stable antiferromagnetic structure appears to be G type. However, an inspection of Table IV shows that in the $\frac{1}{2}(100)$ magnetic structures the important exchange interactions are the short in-plane ones, while the next-nearest-neighbor interplane long exchanges, whether ferromagnetic or antiferromagnetic, have only a minor influence on the total energy and on the Néel temperature. The calculated high Néel points of the C- and G-type structures (466 and 498 K) reflect the presence of the four over six Fe-O-Fe bonds and can be compared to the Néel point of about 750 K expected if all the six first neighbors of a given Fe are Fe too. This scenario reminds the case of $KNiF_3$ and K_2NiF_4, for which the ratio of the Néel temperatures is almost exactly the same as the ratio of nearest-neighbor numbers (i.e., 6/4), as it might be expected if the short path Ni-F-Ni superexchange was responsible for the antiferromagnetic order in both cases.[73]

In disordered samples of PFT, in which N octahedral sites are statistically occupied by $N/2$ Fe and $N/2$ Ta, the most likely local coordination will be a central Fe surrounded by three Fe and three Ta, and therefore the Néel temperature should be further reduced with respect to those of the $\frac{1}{2}(100)$ ordered variant in which each Fe is surrounded by four in-plane Fe and two out-of-plane Ta. However, the evaluation of how the actual distribution of Fe and Ta on B sites might influence on the transition temperatures of real samples of PFT is obviously beyond the aim of our study.

V. ELECTRONIC PROPERTIES

In order to discuss the electronic properties of $PbFe_{1/2}Ta_{1/2}O_3$, in Fig. 6 we plot the corresponding partial densities of states (PDOS), as calculated within LSDA and LSD+U using the $\frac{1}{2}(111)$ cation ordering in the type-I antiferromagnetic structure. The inability of LSDA to describe the electronic structure of strongly correlated systems is well known. In fact the LSDA calculations incorrectly give a metallic behavior, with the Fe spin down bands producing a narrow peak around E_F. Furthermore the spin up and spin down Fe peaks are separated by only ≈ 0.8 eV, related to the exchange interaction strength. We note that this value is underestimated with respect to the one of about 2–3 eV usually obtained with similar calculations.[60,72] We have verified that this is a consequence of the values of the lattice parameters and relaxed internal geometry calculated within LSDA and used in the LSD calculations. As already pointed out in Sec. IV C the LSD theoretical lattice constants are smaller by about 3% than the experimental ones. We notice that by performing LSD calculations using the experimental lattice parameters, that correctly evaluate the spin splitting (about 2.4 eV) as shown in Fig. 6(b), we have found that the LSD internal optimized geometry differs substantially from the one obtained by doing a fully *ab initio* calculation in which relaxed lattice constants were used. In particular, the Fe-O1 and Fe-O2 bond lengths decrease by ≈ 0.1 Å and become shorter than the Ta-O bond length.

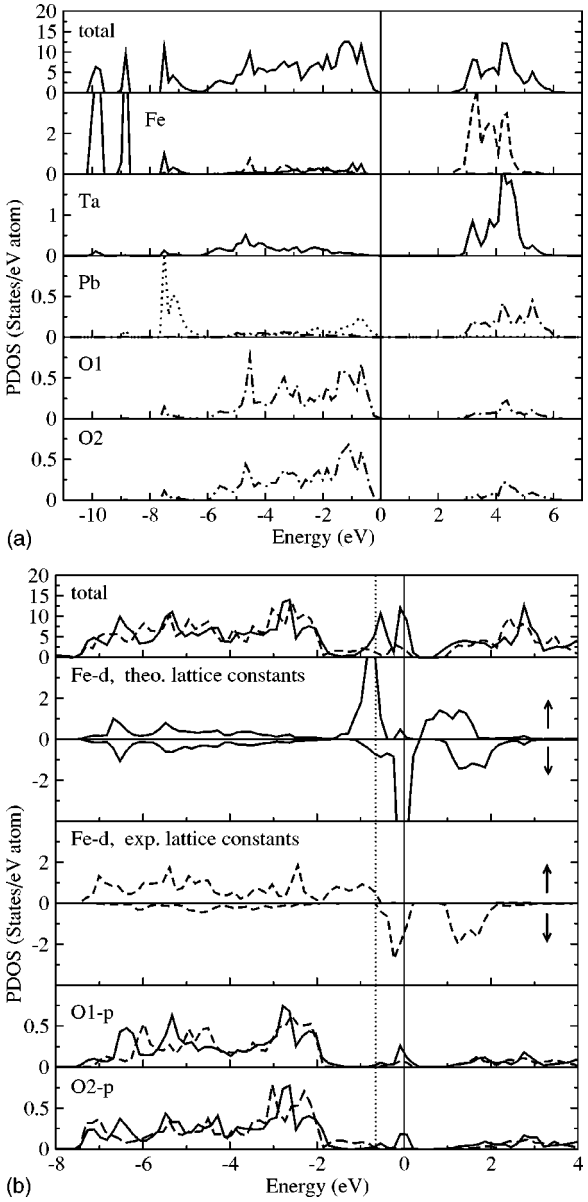

FIG. 6. Total (TDOS) and atom resolved l-decomposed density of states (LDOS) of type-I $\frac{1}{2}(111)$ within (a) LSD+U and (b) LSD approximations. In the LSD+U LDOS plots (a) full, dot-dashed, and dotted lines represent d, p, and s states, respectively. For Fe both majority (full) and minority (dashed) d states are plotted. In (b) the superimposition of LSD LDOS calculated using theoretical (full line) and experimental (dashed) lattice constants is given, both plotted by taking the center of mass of the Pb s states as energy references. The LDOS of Pb and Ta are not drawn. The Fermi level for both theoretical (full) and experimental (dotted) case is drawn. For Fe the majority and minority d states are plotted in two separate panels.

The introduction of the Coulomb interaction term, within

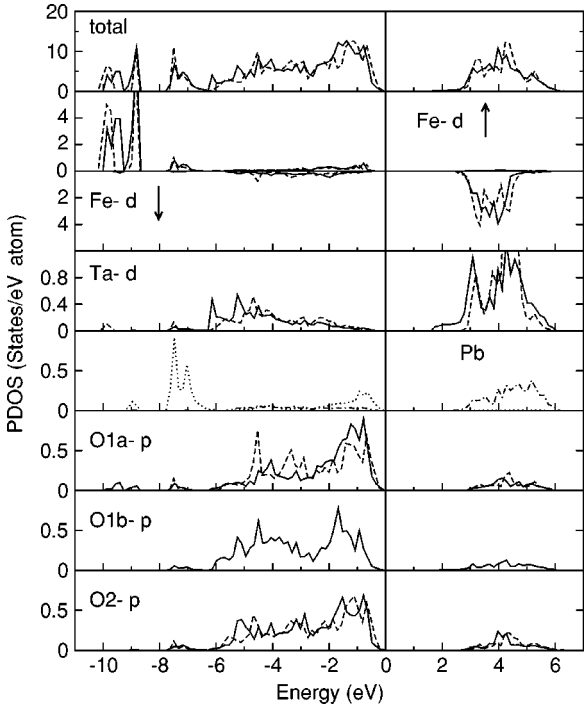

FIG. 7. Comparison between total and partial density of states between type-I $\frac{1}{2}(111)$ (dashed lines) and C-type $\frac{1}{2}(100)$ (full lines) models calculated within the LSD+U approximation. Pb states remain unchanged therefore only *s* (dotted line) and *p* (dot-dashed line) densities for the C-type $\frac{1}{2}(100)$ structure are plotted.

the LSD+U method, opens up a large separation between the spin up and spin down peaks, leading to a gap of about 2.2 eV, between the valence band maximum (with a O1 $2p$ character) and the conduction band bottom (with a dominant Fe character, 50%, hybridized with Ta *d* states, 30%). The lower Fe Hubbard band is found at about -10 to -9 eV below the O $2p$ valence band top. Our results identify this system as a charge transfer insulator, according to Zaanen, Sawatzky, and Allen.[74] The inclusion of correlation also decreases the Fe *d*-band-width. Interestingly, as already pointed out, within LSD+U the Fe spin down component is located at the same energy of the Ta *d* bands, with a non-negligible interaction, crucial in understanding the differences between the two structural variants as will be discussed soon. The hybridization between Fe $3d$ and O $2p$ bands is weak within LSD+U and, obviously, larger within the local density approximation. The Pb $6p$ band is empty, while the $6s$ states are fully occupied and interact, weakly, with the O states near the valence band maximum. It would be interesting to compare our results with photoemission experiments, which are unfortunately not available for this compound. The electronic properties of the two magnetic structures show only minor differences. In particular, in the type-II phase, that is found to be the most stable as reported in Table II, the gap is by ≈ 0.1 eV larger than in the type-I phase.

In order to investigate the influence of Fe-Ta ordering on the electronic structure, we plot in Fig. 7 the PDOS for the $\frac{1}{2}(111)$ and $\frac{1}{2}(100)$ structures, in the type-I and C-type magnetic structures, respectively, as obtained within the LSD+U method. The cation ordering does not bring about major changes, with a few notable differences. The most important difference is found in the Ta *d*-band-width, which is larger in the $\frac{1}{2}(100)$ case. In particular, the presence of a square planar Ta-O1b arrangement allows for a bonding optimization and, therefore, a larger Ta bandwidth. Also, the Ta *d* band is not affected by the Hubbard *U* being the Ta-O1b plane far from the Fe-O1a plane where the Coulomb correlation takes place. As a consequence, in the $\frac{1}{2}(100)$ structure the energy gap is between the oxygen valence band maximum and the Ta conduction band minimum and, as shown in Fig. 1, remains unchanged when *U* increases from 3 to 9 eV. In the $\frac{1}{2}(111)$ case, on the other hand, the presence of mixed Fe-Ta planes allows the Fe-Ta bonding formation. This feature is confirmed by the analysis of angular momentum decomposition of the charge: in $\frac{1}{2}(111)$ going from $U=3$ to 9 eV we find a transfer of 0.12 electron from Ta and O1 to Fe, while in $\frac{1}{2}(100)$ this transfer is absent.

TABLE V. Ferroelectric distortions (i.e., vertical buckling) of the type-I $\frac{1}{2}(111)$ structure. The ferroelectric phase is by 13 meV (per formula unit) more stable than the corresponding paraelectric phase. Distances are given in Å (in brackets the values are written in internal units).

Atoms	Theory (LSD+U)	Expt (Ref. 28)
$b_{[Pb-O2]}$	0.197 (0.025)	0.148 (0.019)
$b_{[Fe/Ta-O1]}$	0.090 (0.011)	0.100 (0.013)

A. Ferroelectricity

We finally investigated the existence of a ferroelectric phase in our computational models of $PbFe_{1/2}Ta_{1/2}O_3$. Our aim here is to investigate if the two cationic arrangements considered have ferroelectric distortions. Therefore we discuss only ferroelectric tetragonal distortions in the C-type $\frac{1}{2}(100)$ and type-I $\frac{1}{2}(111)$ structures (the smallest cell of each variant), to be compared with the first structural symmetry breaking experimentally observed in PFT.

To this end we have used the same lattice constants employed in the paraelectric calculations, even if a fully satisfactory analysis should take into account the elongation of the *c* parameter due to the ferroelectric distortions, as claimed by experiments. In order to allow for ferroelectric distortions we have broken the crystallographic inversion symmetry by imposing small shifts of Pb and O atoms along the *z* axis with respect to the fixed framework of the octahedra, with the origin kept on the Fe atom at $(0,0,0)$. Then, we relaxed the atomic positions. As a consequence the point symmetry of both structures changes to 4 mm.

In the $\frac{1}{2}(100)$ variant we do not find any ferroelectric distortion, while in the $\frac{1}{2}(111)$ structure a polar phase is found to be more stable than the paraelectric one by 26 meV, with ferroelectric distortions in good agreement with experimental values as reported in Table V. In our calculations the *xy* planar coordinates are not affected by the ferroelectric distortions that involve only the *z* direction and, therefore, any possible tilting of the octahedra has been neglected. This

is justified for the hypothetically elpasolite-type perovskite Pb_2FeTaO_6 because the tolerance t factor,[16] defined as $R_A + R_O = t\sqrt{2}(R_B + R_O)$ where R_A, R_B and R_O are the ionic radii in ABO_3, is very close to 1 for both Fe and Ta. This favors phase transitions without rotation of the BO_6 octahedra.

With respect to the paraelectric phase, we find an upward displacement of 0.09 Å for O1 from the Fe-O1-Ta plane at $z=0$. A very similar situation is found for the O1 atom at $z=0.5$ where to an upward displacement of 0.085 Å for O1, follows a downward displacement of 0.004 Å for Fe and Ta. As a result, a net buckling of 0.09 Å between O1 and the metal species is found, as that calculated at $z=0$, and both are in good agreement with the experimental findings (0.100 Å). The atomic species experiencing the largest shifts are the Pb atoms (sited at $z=0.25$ and 0.75). This is consistent with the widely discussed idea that a large portion of the ferroelectric polarization in Pb-based complex perovskites, whether ordered or disordered, is provided by Pb displacements to accommodate the lone-pair $6s^2$ electrons. In our calculations Pb atoms move towards the Fe-O1-Ta plane by 0.162 Å, while the coplanar apical oxygens O2 undergo a displacement by 0.035 Å in the opposite direction, with a buckling of 0.197 Å, larger than the measured value by ≈ 0.05 Å.

We now discuss the changes induced by the ferroelectric displacements on the Néel temperature for the type-I and -II $\frac{1}{2}(111)$ structure. We notice that the total energies of the ferroelectric type-I and ferromagnetic structures are smaller by 26 and 20 meV than those of the corresponding paraelectric phases listed in Table II. A fully satisfactory analysis would require the study of ferroelectricity in the type-II $\frac{1}{2}(111)$ structure, to be simulated by a unit cell containing 80 atoms with very low symmetry. Given the computational effort involved, however, we did not perform this calculation. Given these limitations, we cannot quantify the influence of ferroelectricity on T_N. Our calculations show, however, that for the ferromagnetic and type-I antiferromagnetic structure the corrections differ by ≈ 6 meV, which is of the same order of magnitude of total energy differences between different magnetic orderings. This suggests that the effect should actually be taken into account, in order to estimate such a small T_N (9 K).

In order to investigate further the differences between the paraelectric and the ferroelectric phase of the type-I $\frac{1}{2}(111)$ structure, in Fig. 8 we show a superimposition of the corresponding total and partial densities of states. Even if the total densities of states of the two phases almost coincide (the gap remains unchanged), there are a few differences that directly follow from the geometrical changes due to the ferroelectric distortions. In particular, the peaks at around -4.8 eV for Ta, Fe, O1, and O2 are enhanced in the ferroelectric PDOS and, only for O1, slightly shifted towards lower energies; also we have a larger hybridization between Pb and Fe at around -7.5 eV. This is a consequence of the different bonding picture in the polarized phase, in which Fe/Ta and O1 atoms are no more coplanar and where the vertical distances between the different atoms change significantly. In fact, the changes in the ferroelectric phase found at

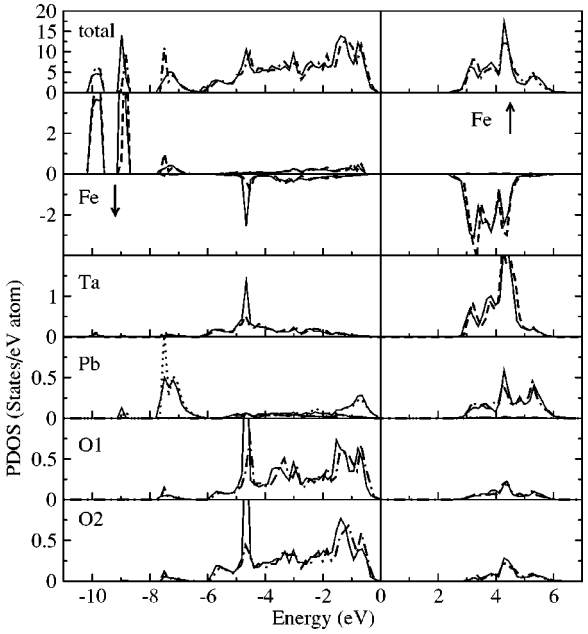

FIG. 8. Comparison between total and partial densities of states between the nonferroelectric and ferroelectric phases of type-I $\frac{1}{2}(111)$. Dashed, dot-dashed, and dotted lines represent *d*, *p*, and *s* states of the paraelectric phase, respectively, while full lines are the corresponding superimposed ferroelectric states.

-4.8 eV involve the d_{z^2} states of Fe and Ta and the p_z states of apical O2, whose stronger hybridization gives more stability to the structure in the ferroelectric phase. The shift of ≈ 0.1 eV of the O1 peak highlights the different bonding between O1 and Fe/Ta due to the buckling between the metal species and the planar oxygen O1 occurring after the phase transition. The changes involves the p_x and p_y states of the planar oxygen that more than the others are affected by the modifications of the electrostatic surrounding due to the displacements.

VI. SUMMARY

In conclusion, we report electronic structure calculations for the multiferroic ferromagnetoelectric perovskite $PbFe_{1/2}Ta_{1/2}O_3$, within the LSD and the LSD+U approximations. The relationships between crystallographic B-site ordering and magnetic properties have been studied in detail for two crystallographic superstructures of the B-site disordered $Pm\bar{3}m$ phase. Our analysis, in particular, explains the experimental reports of two very different magnetic ordering temperatures. The values of Néel temperature, computed for artificially ordered structures, underline the link between short range cation coordination and magnetic properties.

We have found a stable antiferromagnetic phase for an elpasolite-type PFT which sustain ferroelectric tetragonal distortions with large shifts of Pb atoms, in agreement with the fact that a large portion of the ferroelectric polarization in Pb-based complex perovskites is provided by Pb displacements.

ACKNOWLEDGMENTS

We thank A. Filippetti for helpful discussions. This work was partially supported by a supercomputing grant at Cineca (Bologna, Italy) through the Istituto Nazionale di Fisica della Materia (INFM). We also thank the Technical University of Vienna for the use of computer time.

[1] H. Schmid, Ferroelectrics **162**, 317 (1994).
[2] M. Fiebig, Th. Lottermoser, D. Fröhlic, A.V. Goldzev, and R.V. Pisarev, Nature (London) **419**, 818 (2002).
[3] R.E. Newnham and L.E. Cross, Ferroelectrics **12**, 43 (1976).
[4] D.N. Astrov, Zh. Éksp. Teor. Fiz. **49**, 1019 (1965) [Sov. Phys. JETP **11**, 708 (1966)].
[5] G.T. Rado and V.J. Folen, J. Appl. Phys. **33S**, 1126 (1962).
[6] G.A. Smolenskii, A.I. Agranovskaia, S.N. Popov, and V.A. Isupov, Sov. Phys. Tech. Phys. **3**, 1981 (1958).
[7] G.A. Smolenskii, V.A. Isupov, and A.I. Agranovskaya, Fiz. Trend Tela (Leningrad) **1**, 170 (1959) [Sov. Phys. Solid State **1**, 150 (1959)].
[8] G.A. Smolenskii, A.I. Agranovskaia, and V.A. Isupov, Fiz. Trend. Tela (Leningrad) **1**, 990 (1959) [Sov. Phys. Solid State **1**, 907 (1959)].
[9] R.E. Cohen, Nature (London) **358**, 136 (1992).
[10] N.A. Hill and K.M. Rabe, Phys. Rev. B **59**, 8759 (1999).
[11] N.A. Hill, J. Phys. Chem. B **104**, 6694 (2000).
[12] A. Filippetti and N.A. Hill, Phys. Rev. B **65**, 195120 (2002).
[13] M. Fiebig, T. Lottermoser, D. Fröhlich, A.V. Goltsev, and V. Pisarev, Nature (London) **419**, 818 (2002).
[14] G.A. Samara, Solid State Phys. **56**, 240 (2001).
[15] P. Woodward, R.D. Hoffmann, and A.W. Sleight, J. Mater. Res. **9**, 2118 (1994).
[16] F.S. Galasso, *Perovskite and High T_C Superconductors* (Gordon and Breach, New York, 1990).
[17] A.A. Bokov, N.P. Protsenko, and Z.-G. Ye, J. Phys. Chem. Solids **61**, 1519 (2000).
[18] G. Baldinozzi, Ph. Sciau, and J. Lapasset, Phys. Status Solidi A **133**, 17 (1992).
[19] G. Baldinozzi, Ph. Sciau, and P.-A. Buffat, Solid State Commun. **86**, 541 (1993).
[20] C.A. Randall, S.A. Markgraf, A.S. Bhalla, and K.Z. Baba-Kishi, Phys. Rev. B **40**, 413 (1989).
[21] A. Kania and M. Pawelczyk, Ferroelectrics **124**, 261 (1991).
[22] K.Z. Baba-Kishi, G. Cressey, and R.J. Cernik, J. Appl. Crystallogr. **25**, 477 (1992).
[23] C. Malibert, B. Dkhil, J.M. Kiat, D. Durand, J.F. Bérar, and A. Spasojevic-de Biré, J. Phys.: Condens. Matter **9**, 7485 (1997).
[24] N. Setter and L.E. Cross, J. Appl. Phys. **51**, 4356 (1980).
[25] L.E. Cross, Ferroelectrics **151**, 305 (1994).
[26] N. Lampis, Ph. Sciau, and A. Geddo Lehmann, J. Phys.: Condens. Matter **11**, 3489 (1999).
[27] A. Geddo Lehmann and Ph. Sciau, J. Phys.: Condens. Matter **11**, 1235 (1999).
[28] N. Lampis, Ph. Sciau, and A. Geddo Lehmann, J. Phys.: Condens. Matter **12**, 2367 (2000).
[29] A. Geddo Lehmann, F. Kubel, and H. Schmid, J. Phys.: Condens. Matter **9**, 8201 (1997).
[30] W. Brixel, Ph.D. thesis, Genève University (Suisse), 1987.
[31] P. Raevski, V.V. Eremkin, V.G. Smotrakov, M.A. Malitskaya, S.A. Bogatina, and L.A. Shilkina, Crystallogr. Rep. **47**, 1007 (2002).
[32] L.I. Shvorneva and Yu.N. Venevtsev, Zh. Éksp. Teor. Fiz. **49**, 1038 (1965) [Sov. Phys. JETP **22**, 722 (1965)].
[33] S. Nomura, H. Takabayashi, and T. Nakagawa, Jpn. J. Appl. Phys. **7**, 600 (1968).
[34] N. Lampis, Ph.D. thesis, Cagliari University (Italy), 2001.
[35] S.A. Ivanov, S. Eriksson, N.W. Thomas, R. Tellgren, and H. Rundlof, J. Phys.: Condens. Matter **13**, 25 (2001).
[36] S.A. Ivanov, R. Tellgren, H. Rundlof, N.W. Thomas, and S. Ananta, J. Phys.: Condens. Matter **12**, 2393 (2000).
[37] W. Brixel, J.-P. Rivera, A. Steiner, and H. Schmid, Ferroelectrics **79**, 201 (1988).
[38] G. Sághi-Szabó, R.E. Cohen, and H. Krakauer, Phys. Rev. B **59**, 12 771 (1999).
[39] B.P. Burton and E. Cockayne, Phys. Rev. B **60**, R12 542 (1999).
[40] R. Hemphill, L. Bellaiche, A. Garcia, and D. Vanderbilt, Appl. Phys. Lett. **77**, 3642 (2000).
[41] H. Gui, X. Zhang, and B. Gu, J. Phys.: Condens. Matter **8**, 1491 (1996).
[42] M. Weinert, E. Wimmer, and A.J. Freeman, Phys. Rev. B **26**, 4571 (1982).
[43] G. Kresse and J. Furthmüller, Phys. Rev. B **54**, 11 169 (1996).
[44] P.E. Blöchl, Phys. Rev. B **50**, 17 953 (1994).
[45] G. Kresse and D. Joubert, Phys. Rev. B **59**, 1758 (1999).
[46] J.P. Perdew and A. Zunger, Phys. Rev. B **23**, 5048 (1981).
[47] M. Imada, A. Fujimori, and Y. Tokura, Rev. Mod. Phys. **70**, 1039 (1998).
[48] V.I. Anisimov, J. Zaanen, and O.K. Andersen, Phys. Rev. B **44**, 943 (1991).
[49] A.B. Shick, A.I. Liechtenstein, and W.E. Pickett, Phys. Rev. B **60**, 10 763 (1999).
[50] S.L. Dudarev, G.A. Botton, S.Y. Savrasov, C.J. Humphreys, and A.P. Sutton, Phys. Rev. B **57**, 1505 (1998).
[51] M. Posternak, A. Baldereschi, S. Massidda, and N. Marzari, Phys. Rev. B **65**, 184422 (2002).
[52] W.E. Pickett, S.C. Erwin, and E.C. Ethridge, Phys. Rev. B **58**, 1201 (1998).
[53] J. Zaanen and G.A. Sawatsky, J. Solid State Chem. **88**, 8 (1990).
[54] A.E. Bocquet *et al.*, Phys. Rev. B **46**, 3771 (1992).
[55] T. Saitoh, A.E. Bocquet, T. Mizokawa, and A. Fujimori, Phys. Rev. B **52**, 7934 (1995).
[56] I. Solovyev, N. Hamada, and K. Terakura, Phys. Rev. B **53**, 7158 (1996).
[57] Z. Yang, Z. Huang, L. Ye, and X. Xie, Phys. Rev. B **60**, 15 674 (1999).
[58] T. Mizokawa and A. Fujimori, Phys. Rev. B **54**, 5368 (1996).
[59] H. Wu, Phys. Rev. B **64**, 125126 (2001).
[60] Z. Fang, K. Terakura, and J. Kanamori, Phys. Rev. B **63**, 180407(R) (2001).
[61] K. Miura and K. Terakura, Phys. Rev. B **63**, 104402 (2001).

[62] V.I. Anisimov, I.S. Elfimov, N. Hamada, and K. Terakura, Phys. Rev. B **54**, 4387 (1996).
[63] J.S. Smart, Phys. Chem. Solids **11**, 97 (1959).
[64] G.H. Jonker, Physica (Amsterdam) **22**, 707 (1956).
[65] D.D. Sarma, N. Shanthi, S.R. Barman, N. Hamada, H. Sawada, and K. Terakura, Phys. Rev. Lett. **75**, 1126 (1995).
[66] P.W. Anderson, Phys. Rev. **79**, 705 (1950).
[67] R.I. Hines, N.L. Allan, G.S. Bell, and W.C. MacKrodt, J. Phys.: Condens. Matter **9**, 7105 (1997).
[68] M.E. Lines, Phys. Rev. A **139**, A1304 (1965).
[69] Encyclopedia of Physics, edited by S. Flugge and H.P.J. Wijn (Springer-Verlag, Berlin, 1966), Vol. XVIII/2 (Magnetism).
[70] D. Kodderitzsch, W. Hergert, W.M. Temmerman, Z. Szotek, A. Ernst, and H. Winter, Phys. Rev. B **66**, 064434 (2002).
[71] J.E. Pask, D.J. Singh, I.I. Mazin, C.S. Hellberg, and J. Kortus, Phys. Rev. B **64**, 024403 (2001).
[72] I.V. Solovyev, Phys. Rev. B **65**, 144446 (2002).
[73] E. Legrand and R. Plumier, Phys. Status Solidi **2**, 317 (1962).
[74] J. Zaanen, G.A. Sawatzky, and J.W. Allen, Phys. Rev. Lett. **55**, 418 (1985).